Miniaturized multiple Fourier-horn ultrasonic droplet generators for biomedical applications†

Chen S. Tsai,*[a] Rong W. Mao,[a] Shih K. Lin,[a] Ning Wang[a] and Shirley C. Tsai[b]

Received 29th April 2010, Accepted 17th June 2010
DOI: 10.1039/c005262k

Here we report micro-electro-mechanical system (MEMS)-based miniaturized silicon ultrasonic droplet generators of a new and simple nozzle architecture with multiple Fourier horns in resonance but without a central channel. The centimetre-sized nozzles operate at one to two MHz and a single vibration mode which readily facilitates temporal instability of Faraday waves to produce monodisperse droplets. Droplets with diameter range 2.2–4.6 μm are produced at high throughput of 420 μl min^{-1} and very low electrical drive power of 80 mW. We also report the first theoretical prediction of the droplet diameter. The resulting MHz ultrasonic devices possess important advantages and demonstrate superior performance over earlier devices with a central channel and thus have high potential for biomedical applications such as efficient and effective delivery of inhaled medications and encapsulated therapy to the lung.

I. Introduction

A variety of droplet (or drop) generation devices based on acoustic techniques have been realized for various potential applications in recent years. For example, nozzleless droplet ejectors that utilize 5–300 MHz focused acoustic beams to eject 300–5 μm water droplets,[1] and that utilize 300–900 MHz focused acoustic waves *via* micro-machined self-focusing transducer to eject 80–5 μm water droplets,[2] one drop at a time, are applicable to high-resolution ink-jet printing. Micro-machined flextensional 2-D droplet ejector arrays with 4 and 10 μm orifices at 3.45 and 2.15 MHz, respectively, produce water droplets[3] for potential applications to biomedicine and biotechnology. A micro-machined 2-D droplet ejector array using a liquid horn structure[4–6] is capable of ejecting 7.2 μm droplets from a 5.9 μm orifice at a resonant frequency of 0.95 MHz,[5,6] and has been shown applicable to drug and gene delivery.[7] Based on the reported data, the 5–7 μm-diameter droplet throughputs of the aforementioned devices are in the order of 12 μl min^{-1} or lower per ejector. Clearly, a much higher droplet throughput can be achieved by the aforementioned 2-D array ejectors. The droplet generator using surface acoustic waves at 20 MHz produced droplets with a broad size distribution at a throughput up to 200 μl min^{-1} and was employed to study the twin-stage impinger model for inhalation drug delivery.[8] Finally, ultrasonic nebulizers[9,10] that utilize a micron-sized vibrating mesh sieve produce droplets with throughput ranging from 160 to 400 μl min^{-1} over a large size range (1 to >10 μm) because various atomization mechanisms are involved.

Here we show the new MEMS-based miniaturized ultrasonic droplet generators (also called nozzles interchangeably for convenience) that utilize the temporal instability of MHz Faraday waves and multiple Fourier horns in resonance to produce 2.2–4.6 μm monodisperse droplets at a high throughput of 420 μl min^{-1} and very low electrical drive power of 80 mW. Specifically, Section II presents a summary of the physical mechanism, *i.e.* temporal instability of Faraday waves, for generation of monodisperse droplets, theoretical predictions of droplet diameter, and the relevant design rules of the droplet generators. Section III describes the new architecture of the silicon-based ultrasonic droplet generators, their design, simulation, and fabrication. Section IV presents detailed results of atomization experiments, following a brief description of the experimental setup and methods, and compares them to the theoretical predictions and the performance of most advanced commercial nebulizers. Section V discusses the imminent applications of the MHz droplet generators to inhalation drug delivery and describes the preliminary experiments with isoproterenol aerosol deposition and human recombinant insulin bioactivity evaluation. Finally, Section VI provides conclusions and suggestions for some potential applications of the MHz ultrasonic droplet generators.

II. Physical mechanism for generation of monodisperse droplets—temporal instability of Faraday waves

Faraday waves, also called standing capillary waves, were first observed forming on the free surface of water on a horizontal support subjected to vertical mechanical vibration by Lord Faraday[11] in 1831 and subsequently analyzed by Lord Rayleigh[12] in 1883. Faraday instability, the underlying physical mechanism for Faraday wave formation and amplification, was studied extensively during the 1990s, but only at very low drive frequency ranging from 6 Hz to 50 kHz.[13–18] Furthermore, no definitive relationship between Faraday instability and atomization (or droplet generation) was reported in these earlier studies. Recently, we studied Faraday instability at MHz drive

[a]*Dept. of Elec. Eng. and Comp. Science and Inst. for Surface and Interface Science, University of California, Irvine, CA, 92697, USA. E-mail: cstsai@uci.edu*
[b]*Dept. of Chem. Eng. and Material Science, University of California, Irvine, CA, 92697, USA*

† Electronic supplementary information (ESI) available: Video I. Spray of water droplets from the 2 MHz nozzle. See DOI: 10.1039/c005262k

frequencies for atomization and generation of monodisperse droplets using silicon-based ultrasonic nozzles with a central channel for liquid feeding.[19,20] In this recent work, the temporal instability of MHz Faraday waves was investigated[20] based on the liquid layer resting on the endface of the nozzle tip.

Faraday waves are generated on the free surface of the liquid layer resting on the planar endface of the nozzle tip as shown in Fig. 1A when the peak longitudinal excitation displacement (h) of the endface (at the drive frequency f) reaches a critical value h_{cr}. Since the excitation is a periodic function, the Floquet theory and the Fourier method are applied in the theoretical treatment. Furthermore, for low-viscosity liquids and low vibration amplitudes used in this study, the time-dependent portion of the governing equation is simplified to the Mathieu differential equation. The amplitude $\xi(x,t)$ of the resulting Faraday waves with initial amplitude ξ_o is as follows:[20]

$$\xi(x,t) = \xi_o e^{\pi kf(h - hcr)t} \sin(2\pi(f/2)t - \pi/4)\cos kx \quad (1)$$

where t designates time and $k = 2\pi/\lambda$ is the wave number of the Faraday waves. The frequency of the Faraday waves is seen as equal to one half of the drive frequency, and the corresponding Faraday wavelength λ is determined by the following equation:[21]

$$f^2 = 8\pi\sigma/\rho\lambda^3 + 64\mu^2\pi^2/\rho^2\lambda^4 \quad (2a)$$

$$\lambda = (8\pi\sigma/\rho)^{1/3} f^{-2/3} \quad (2b)$$

where σ, ρ and μ are the surface tension, mass density, and dynamic viscosity of the liquid, respectively. Note that for low viscosity liquids such as water, eqn (2a) reduces to the Kelvin equation, eqn (2b).[22] The Faraday wavelengths at the 1.0–2.0 MHz frequencies of interest here range from 5.7 to 12.2 μm as shown in Table 1.

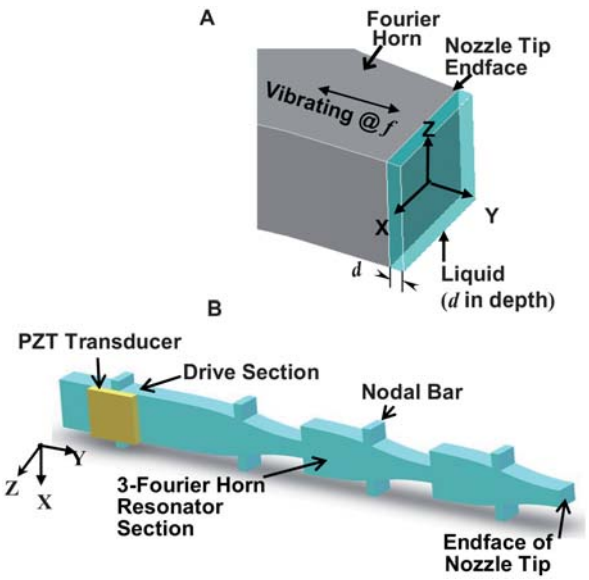

Fig. 1 (A) Geometry of the nozzle endface for initiation of the temporal instability of Faraday waves on the free surface of the liquid layer, and (B) 3-D architecture of the new MHz ultrasonic nozzle with three Fourier horns but without a central channel.

Clearly, the Faraday waves generated become temporally unstable when the peak excitation displacement h exceeds the critical value h_{cr} for Faraday wave formation given as follows:[20]

$$h_{cr} = 2\mu(\pi\rho^2\sigma)^{-1/3} f^{-1/3} \quad (3)$$

In other words, the amplitude of the Faraday waves increases exponentially with time as shown in eqn (1). Note that while h_{cr} decreases with increasing drive frequency, the exponent $\pi kf(h - h_{cr})t$ of the exponential factor in eqn (1) is proportional to 4/3 power of the drive frequency, namely, $f^{4/3}$. Therefore, at the MHz drive frequencies, the amplitude of the Faraday waves grows rapidly once the excitation displacement h exceeds the critical value h_{cr}, and the Faraday waves become unstable, resulting in atomization and production of monodisperse droplets.

Finally, a theoretical formula for the diameter of the droplets produced was established for the first time based on the Rayleigh oscillation.[23] In terms of the Faraday wavelength λ given by eqn (2b), the diameter of the droplet D_p is given as follows:

$$D_p = 2(2/\pi^2)^{1/3}(\sigma/\rho)^{1/3} f^{-2/3} = 0.40\lambda \quad (4)$$

Namely, the droplet diameter equals four tenths of the Faraday wavelength.

In short, eqn (2), (3), and (4) for the key physical quantities provide the design specification for the ultrasonic nozzles fabricated and studied.

III. Nozzle architecture, design, simulation, and fabrication

Nozzle architecture

Fig. 1B shows the three-dimensional (3-D) architecture of a basic ultrasonic droplet generator or nozzle that is composed of a lead zirconate titanate (PZT) transducer drive section and a resonator section with multiple (3 in the example) Fourier horns in a silicon substrate.[19,20] Each Fourier horn is one half-wavelength long with a longitudinal vibration amplitude (displacement) gain of two.[24,25] Two versions of the nozzle architecture have been devised to construct a variety of droplet generators. The earlier version consists of a bonded pair of basic nozzles each with an etched trough to form a 200 μm × 200 μm central channel along the nozzle axis for flow of the liquid to be atomized.[25] The new version reported here (Fig. 2A and 2B) consists of one such basic nozzle (without an etched trough) alone; the liquid to be atomized is externally transported to the nozzle endface. Since the droplet size depends solely on the nozzle design frequency in accordance with eqn (4), both versions of the nozzle architecture produce the same droplet size at the same nozzle drive frequency. However, as the nozzle drive frequency increases beyond 1.0 MHz, it becomes increasingly difficult to fabricate a central channel of sufficient cross sectional area because of the corresponding decrease in nozzle dimensions. Thus, the new version without a central channel has the following important advantages over the earlier version with a central channel: fewer micro fabrication steps, higher drive frequency capability to produce smaller droplets, higher flow rate and droplet throughput, lower electrical drive power for atomization, and less prone to clogging of medicinal solutions. Except for the effects of the number of

Table 1 Measured droplet diameters are in agreement with predicted values of $D_p = 0.40\lambda$

Drive frequency f/MHz (nominal)	Liquid	Surface tension σ (dyn cm^{-1})	Density ρ/g cm^{-3}	Faraday wavelength λ^a/μm	Droplet diameter D_p/μm	
					Predicted 0.40λ	Measured[b]
1.0	Water	72	1.00	12.2	4.88	4.64
1.0	Glycerol (aq.)[c]	72	1.11	11.7	4. 71	4.51
1.0	Alcohol	23	0.79	9.0	3.60	3.47
1.5	Water	72	1.00	9.3	3.72	3.66
1.5	Glycerol (aq.)[c]	72	1.10	9.0	3.59	3.73
1.5	Alcohol	23	0.79	6.9	2.76	2.49
2.0	Water	72	1.00	7.7	3.08	2.89
2.0	Alcohol	23	0.79	5.7	2.27	2.24

[a] Faraday wavelength $\lambda = (8\pi\sigma/\rho)^{1/3}f^{-2/3}$ except with aqueous glycerol where viscosity is taken into account based on eqn (2a) of the text. [b] Experimental errors: ±0.04 for 1.0 and 1.5 MHz; ±0.08 for 2.0 MHz nozzles. [c] Aqueous solution of 40–44 wt% glycerol with viscosity up to 4.5 cP.

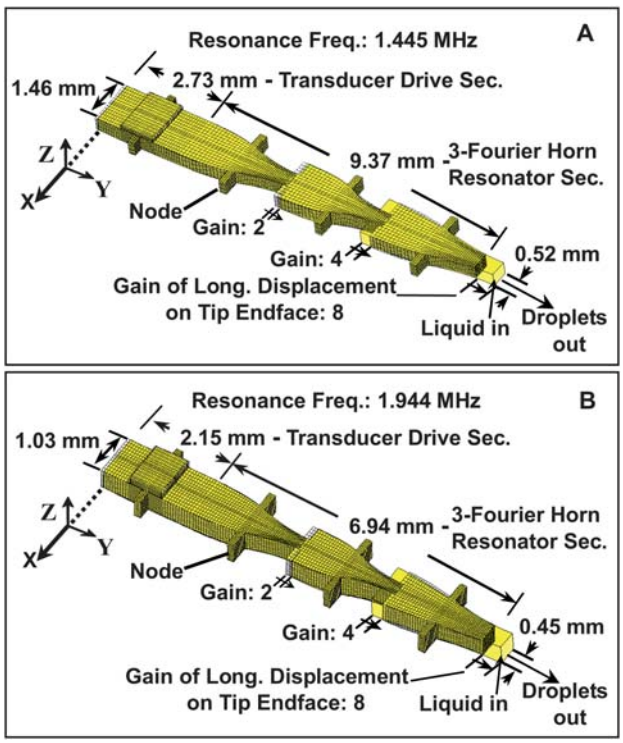

Fig. 2 Simulation results of new nozzles without a central channel: (A) 1.5 MHz and (B) 2.0 MHz. Note the locations of the four vibration nodes to which silicon strips for mechanical support are attached; the mesh lines of the un-deformed nozzles but only the edges of the deformed nozzles are shown; the first and third horns extend while the drive section and the second horn contract during deformation; and the resonance frequencies, determined by ANSYS 3-D simulation for the design (nominal) frequencies of 1.5 and 2.0 MHz, are 1.445 and 1.944 MHz, respectively.

Fourier horns on the electrical drive power measured using the 1.0 MHz nozzle with a central channel, the results reported here were all obtained with nozzles of the new architecture. Notably as depicted in Fig. 1A the endface-liquid configuration with this new nozzle architecture mimics the classical geometry modeled in all theoretical studies of Faraday wave formation and Faraday instability summarized in Section II, namely, a liquid layer of depth d resting on a planar solid support that is subjected to mechanical vibration perpendicular to the free liquid surface.[11–18]

Design and simulation

The nozzle was designed to vibrate in a single longitudinal mode in the direction perpendicular to the endface (Y-axis in Fig. 2A and 2B) at the single resonance frequency of the three Fourier horns. The longitudinal axis of the nozzle (Y-axis) is in the direction of the primary flat, namely, <110> of the silicon wafer with the highest acoustic velocity. A 3-D finite element method (FEM) simulation was carried out using the commercial ANSYS (ANSYS Inc., Canonsburg, PA) Program first for vibration mode shape analysis[25] and then for impedance analysis.[20] The mode shape analysis determines the nozzle resonance frequency of the pure longitudinal vibration mode; the impedance analysis determines the longitudinal vibration displacement on the nozzle endface (tip) and the impedance at the nozzle resonance frequency. Except for application of an alternating current (AC) voltage of 1.0 V to the PZT transducer electrode at the nozzle resonance frequency, the impedance analysis follows procedures similar to those for mode shape analysis.[25] The resulting longitudinal vibration displacement on the nozzle endface is used to determine the voltage required to produce the critical excitation displacement h_{cr} given by eqn (3). The threshold voltage thus obtained together with the resistive part of the impedance is then used to calculate the minimum electrical drive power required for atomization.

The material properties of silicon were taken from the literature,[20,25] and the material properties of the PZT-5H transducer were slightly adjusted based on the published data in the literature and those provided by the PZT manufacturer so that the simulated impedance curve of PZT would match the measured impedance curve.[20] As shown in Fig. 2 for both 1.5 and 2.0 MHz nozzles with three Fourier horns at resonance, the base plane of the down-stream Fourier horn undergoes the same displacement as the tip plane of the neighboring up-stream Fourier horn. As a result, the maximum longitudinal displacement at each succeeding horn tip increases progressively by a factor of 2, resulting in a total gain of 8 (= 2^3) on the endface of the nozzle. The greatly enhanced peak vibration displacement on the nozzle endface at low drive power facilitates the critical vibration displacement required to initiate the temporal instability of the Faraday waves and, thus, atomization.

Both the simulation results with the acoustical and electrical losses taken into account and the experimental results show that the optimum number of Fourier horns in terms of electrical drive

power requirement is 3 or 4. Both 3- and 4-Fourier horn nozzles were fabricated and studied. Their atomization performances were found to be very similar, and the 3-Fourier horn nozzle is used here as an example. For a loss-free 3-Fourier horn nozzle as shown in Fig. 2, the total gain of vibration displacement on the nozzle endface is 8 as mentioned previously. As presented later in Section IV, 1.0 MHz nozzles with one, two, and four Fourier horns with respective total gains of vibration displacement on the endface of 2, 4, and 16 were also fabricated to verify the effect of multiple Fourier horns on the aforementioned essential requirement of peak vibration displacement for initiation of temporal instability of Faraday waves and atomization. It should be emphasized that the single longitudinal-vibration mode at the single resonance frequency of multiple Fourier horns ensures single-mode capillary wave atomization and production of monodisperse droplets. This is in stark contrast to other ultrasonic devices such as conventional ultrasonic nebulizers that involve various atomization mechanisms such as cavitation, impinging, and jetting in addition to capillary wave mechanism with multiple oscillation modes.[9,18,27,28] Simultaneous involvement of multiple atomization mechanisms and/or oscillation modes not only increases the critical vibration amplitude and, thus, the electrical drive power required for atomization, but also drastically broadens the size distribution of the resulting droplets.[18]

In short, the specifications of the new 3-Fourier horn nozzles at 1.0, 1.5, and 2.0 MHz are, respectively: nozzle resonance frequency (in MHz) of 0.971, 1.445, and 1.944; physical dimensions (in cm × cm × cm) of 1.79 × 0.21 × 0.05, 1.20 × 0.15 × 0.05, and 0.85 × 0.11 × 0.05; and droplet diameter (D_p in μm) of 4.88, 3.72, and 3.08 for water.

Fabrication

The silicon-based nozzle was fabricated using MEMS technology.[20,26] The drive and resonator sections of the nozzle were formed in a single-fabrication step using an inductive coupled plasma (ICP) process.[20,25] Note that a large number of nozzles with similar or different design specifications can be fabricated in one batch on a common silicon wafer. Fig. 3A shows such an example. Nozzles at three operating frequencies of interest (1.0, 1.5 and 2.0 MHz) have been realized to produce 2.2–4.6 μm monodisperse droplets. The detailed dimensions and simulation results of the 1.5 MHz and 2.0 MHz nozzles are shown in Fig. 2A and 2B, respectively. Fig. 3B shows a photograph of the nozzles fabricated and studied.

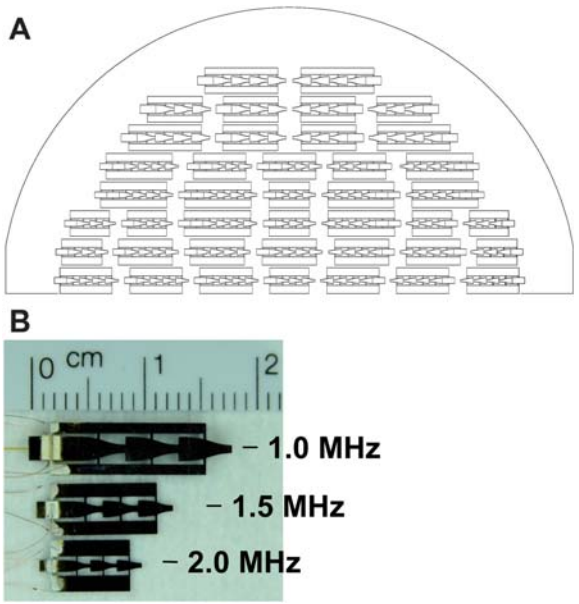

Fig. 3 (A) Layout of different nozzle designs on a half 10 cm-silicon wafer, and (B) a photograph of the new 1.0, 1.5 and 2.0 MHz 3-Fourier horn nozzles fabricated.

IV. Atomization experiments and results, and comparison with theoretical predictions

Experimental setup, methods and materials

All the atomization experiments presented below were conducted using the setup shown in Fig. 4. Major components of the setup are: (i) a PZT transducer drive system to provide a MHz electrical drive to the ultrasonic nozzle, (ii) a syringe pump (*kd* Scientific Model #101) to provide a controlled flow rate of liquid, (iii) a CCD camera to take pictures or movies of the spray produced, and (iv) a Malvern/Spraytec System (Model #STP

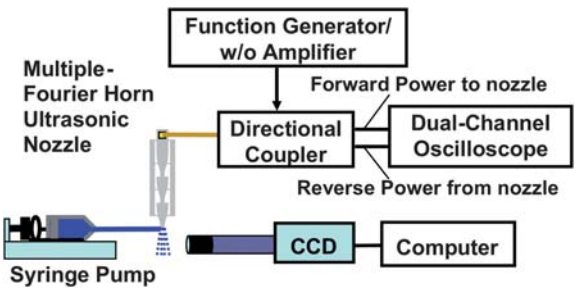

Fig. 4 Schematics of atomization setup.

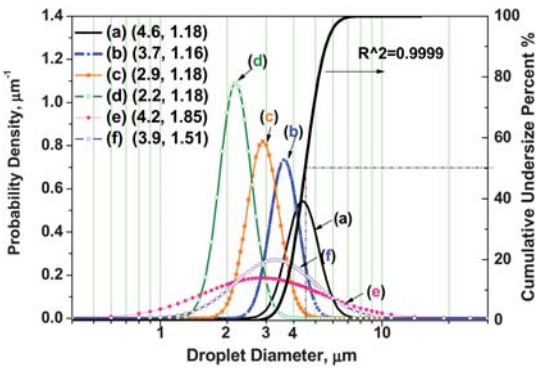

Fig. 5 Comparison of measured droplet sizes and size distributions in logarithmic scale, with MMD/GSD in parentheses for (a) to (d), and MMAD/GSD for (e) and (f): (a) 1.0 MHz nozzle with water (4.6 μm/1.18), (b) 1.5 MHz nozzle with water (3.7 μm/1.16), (c) 2.0 MHz nozzle with water (2.9 μm/1.18), (d) 2.0 MHz nozzle with alcohol (2.2 μm/1.18), (e) Omron NE-U22V (4.2 μm/1.85), and (f) Pari eFlow (3.9 μm/1.51). Note: MMD and MMAD are mass median diameter and mass median aerodynamic diameter, respectively. MMD was obtained in ambient air using the Malvern/Spraytec System while MMAD was obtained in the presence of high-velocity air using a commercial cascade impactor for plots (e) and (f).

5311) for analysis of droplet size and droplet-size distribution (not shown in the figure). The Malvern/Spraytec System is a non-invasive particle sizing instrument based on laser light diffraction. Since the laser beam has a cross sectional area (1 cm in diameter) much larger than the column (spray) of droplets (~0.07 cm × 0.1 cm) produced by the miniaturized nozzle, the data reported in this study were obtained from the entire cross section of the droplet stream. The data include mass median diameter (MMD) and geometrical standard deviation (GSD). GSD and geometric mean of a data set with a log-normal distribution are, respectively, equivalent to the standard deviation and arithmetic mean of a data set with normal distribution. GSD is simply calculated by the geometric mean of quotients (ratios) D_{84}/D_{50} and D_{50}/D_{16}, where D_{84}, D_{50}, and D_{16} are, respectively, the droplet diameters at 84.1%, 50.0%, and 15.9% of the cumulative undersize percent of the droplet size distribution as shown in Fig. 5. Note that the GSD was obtained by least square fit ($R^2 = 0.9999$ as shown in Fig. 5) of the cumulative undersize percentage curve obtained using the Malvern/Spraytec System.

Water and alcohol were used in most of the experiments since they are among the most common solvents used in inhaled drug delivery. In order to study the effect of viscosity, atomization of aqueous solutions of glycerol and lactose with dynamic viscosity up to 4.5 centipoise (cP) were carried out. Aqueous solutions of isoproterenol (β_2-agonist), recombinant human insulin R-100 (molecular weight of 6000 Dalton),[29] and an aqueous dispersion of gold nanoparticles (23–26 nm in diameter)[30] were also successfully atomized. As depicted in Fig. 6, the liquid (water) to be atomized at the drive frequency of 1.445 MHz (Fig. 6A for the 1.5 MHz nozzle) or 1.950 MHz (Fig. 6B for the 2.0 MHz nozzle) was brought to the nozzle endface using a piece of tubing. The water flow rate was varied using the electronically controlled syringe pump. Continuous atomization of water at 1.950 MHz drive frequency using the 2.0 MHz nozzle and external water feeding is shown in Video I.† Both the video and Fig. 6 show that the fine spray of water droplets produced has low momentum. Furthermore, both the profile and the 20–25 μm depth (d in Fig. 1A) of the water layer formed on the nozzle endface remained constant while stable atomization continued for a period of many hours with throughput as high as 420 μl min^{-1} until the electrical drive was turned off. As shown in Fig. 5, the 2.2 to 4.6 μm droplets produced were found to be monodisperse; the corresponding droplet volumes are 6 to 50 femtolitres. Successful production of monodisperse droplets from the model endface geometry of the new nozzle (see Fig. 1A) with various liquids unequivocally verifies the temporal instability of Faraday waves as the mechanism for atomization and generation of monodisperse droplets. It also suggests the potential to produce monodisperse droplets of even smaller sizes by using the same nozzle endface geometry at increased nozzle resonance frequency.

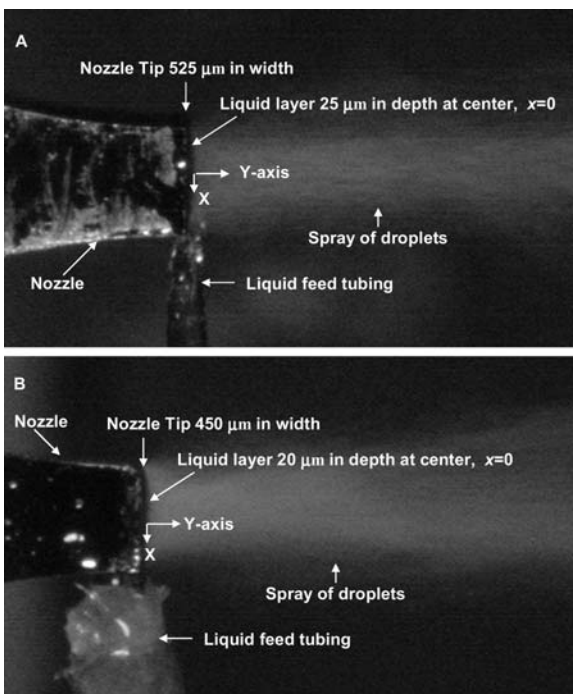

Fig. 6 Water atomization using the MHz 3-Fourier horn ultrasonic nozzles without a central channel but with external feeding onto the nozzle endface: (A) 1.5 MHz at droplet throughput of 350 μl min^{-1} and electrical drive power of 55 mW, and (B) 2.0 MHz at droplet throughput of 420 μl min^{-1} and electrical drive power of 80 mW.

Diameter of droplets and droplet size distribution

Fig. 5 shows the measured size distributions of the droplets produced by atomization with the 1.0, 1.5 and 2.0 MHz nozzles (plots (a), (b), (c), and (d)). The corresponding geometric standard deviations (GSD) of the droplets are shown to be as small as 1.18, 1.16, 1.18, and 1.18, respectively. Note that a GSD of 1.0 corresponds to a single size and that aerosols with a GSD up to 1.22 are commonly accepted as monodisperse in aerosol medicine.[31] For comparison, the size distributions of polydisperse droplets with GSDs of 1.85 (Omron published data sheet) and 1.51 (Pari eFlow)[32] generated by the two most advanced commercial nebulizers are also shown in Fig. 5, plots (e) and (f), respectively. Note that the throughput of such commercial devices ranges from 160 to 400 μl min^{-1}, but with very broad droplet size distributions as described. The Pari eFlow, which utilizes vibrating mesh technology, is capable of high throughput but also suffers from broad droplet size distribution (GSD > 1.5) and clogging of the orifices that are considerably smaller in diameter than the droplets produced.[33]

The validity of the theoretical formula, eqn (4), is confirmed by its close agreement with the measured droplet diameters listed in Table 1. For example, the diameters of water and alcohol droplets produced by the 2.0 MHz nozzle measure 2.89 and 2.24 μm, respectively, while the corresponding theoretical diameters are 3.08 and 2.27 μm. Also, the effect of viscosity on the droplet diameter was found to be less than 3% for aqueous solutions of glycerol and lactose with viscosity up to 4.5cP as predicted by the lack of viscosity term in the theoretical formula of eqn (2). These findings establish the first theoretical formula for the diameter of droplets generated by single-mode capillary wave atomization.

Electrical drive power required for atomization

As shown in Fig. 4, the PZT drive system consists of a MHz function generator with or without an amplifier and a −50 dB

directional coupler that taps 10^{-5} of the input power to the oscilloscope for measurement.[20,25] The MHz voltage is applied to the PZT transducer to activate the ultrasonic nozzle. The directional coupler has two taps: the forward power tap for monitoring the incident power from the generator and the reverse power tap for monitoring the reflected power from the nozzle. The tapped or coupled voltage is connected *via* a 50 Ω coaxial cable to a dual-channel oscilloscope for measuring the peak-to-peak voltage (V_{pp}) of the corresponding incident voltage to the nozzle and the corresponding reflected voltage from the nozzle, respectively. The power measured at each tap is equal to $V_{pp}^2/8Z$, where Z (= 50 Ω) is the impedance of the coaxial cable. Note that the directional coupler incurs negligible power loss at the frequency range of interest. The actual power consumed by the nozzle during atomization is equal to the power measured at the forward power tap subtracted by that measured at the reverse power tap caused by mismatch between the nozzle impedance and the 50 Ω of the coaxial cable, and then multiplied by the factor of 10^5 which corresponds to the 10^{-5} tapping of the −50 dB (10^{-5}) directional coupler used.

The measured electrical drive power *versus* droplet throughput curves for the 1.5 and 2.0 MHz nozzles are shown in Fig. 7. The figure shows a threshold drive power as low as 20 mW at low throughput and increasing moderately to 55 mW at high throughput of 350 μl min^{-1} for the 1.5 MHz nozzle. Similar characteristics are also provided in Fig. 7 for the 2.0 MHz nozzle but at the higher drive power of 73 mW at a throughput of 350 μl min^{-1}. For the 1.0 MHz nozzle, although the measured threshold drive power was comparable, the drive power of 120 mW at the throughput of 350 μl min^{-1} was much higher. The measured threshold drive powers of 20 mW for the 1.5 MHz nozzle and 50 mW for the 2.0 MHz nozzle at low droplet throughput are in reasonable agreement with the respective simulated minimum powers of 16 and 26 mW required for atomization. As described previously in the specific simulation procedures employed, the simulated minimum drive power is calculated in accordance with eqn (3), but does not take into account the power loss due to the bonding layer between the PZT transducer and the silicon base of the drive section in the fabricated nozzles.

Furthermore, the critical vibration displacement h_{cr} of 0.33, 0.29 and 0.26 μm predicted by eqn (3) for water at 1.0, 1.5, and 2.0 MHz drive frequencies, respectively, are to be compared to the measured peak excitation displacements of 0.34, 0.32, and 0.31 μm required for atomization using a laser Doppler vibrometer

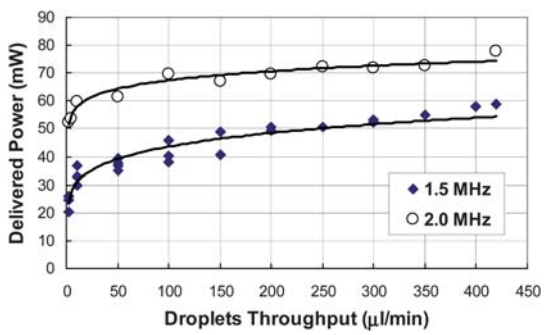

Fig. 7 Measured electrical drive power delivered to the 1.5 and 2.0 MHz 3-Fourier horn nozzles during atomization of water for production of monodisperse droplets.

Table 2 Simulation results of minimum (threshold) electrical drive power required for atomization *versus* PZT transducer thickness and number of Fourier horns[a]

Drive frequency/MHz	1.0[b]		1.5[b,c]		2.0[c]
PZT thickness/μm	400	200	200	200	200
Number of Fourier horns	Electrical drive power/mW				
1	315	66	120[b]	60[c]	143
2	100	30	47[b]	23[c]	49
3	36	22	30[b]	16[c]	26
4	28	21	28[b]	15[c]	22

[a] Effect of bonding layer between PZT and silicon not included. [b] With a central channel. [c] Without a central channel.

(Polytech GmbH, Model PSV 400). The fact that the measured peak excitation displacements are only slightly higher than the predicted h_{cr} values verifies the conclusion made earlier in Section II that the MHz Faraday waves rapidly become unstable and result in atomization once the excitation displacement exceeds the critical vibration displacement. Thus, the low peak excitation displacements required for atomization support the low electrical drive power measured for atomization, namely, 73, 55, and 120 mW at throughput of 350 μl min^{-1} with the 2.0, 1.5, and 1.0 MHz nozzles, respectively. Note that the power required for the 1.0 MHz nozzle is significantly higher than those for the 1.5 and 2.0 MHz nozzles because a PZT transducer thickness of 400 μm was used for the former while a transducer thickness of 200 μm was used for the latter. Simulation results presented in Table 2 clearly show that the electrical loss associated with the lossy PZT transducer increases with its thickness. Table 2 also shows that the nozzles with a central channel require higher drive power for atomization. The higher drive power is attributable to the requirement of a pair of PZT transducers (one each for the pair of basic nozzle) for their activation. Also note that the range of drive power measured is at least two orders of magnitude lower than that required in conventional ultrasonic atomization using MHz disk transducers.[34] This very low drive power requirement is attributable to the resonance effect of the three Fourier horns used in the nozzles, since only a minute amount of power is needed to excite a nearly loss-free resonant system.

The major sources of power losses that must be furnished by the electrical generator are the vibration of the nozzle endface, the lossy PZT transducer, and the bonding between the PZT transducer and the silicon base in the drive section. As presented in Table 2, the required power associated with the first source is calculated to be 16 mW at a peak excitation displacement of 0.29 μm for the 1.5 MHz nozzle, while the power required to account for the surface energy of 2.5 μm droplets at throughput of 350 μl min^{-1} is negligible (<1 mW). Thus, the much lower power requirements of all the new nozzles reported here in comparison to those of the earlier nozzles are largely attributed to the new nozzle architecture requiring only a single basic nozzle without a central channel and, thus, a single PZT transducer for activation.

Effect of multiple Fourier horns on drive power requirement

Simulation results presented in Table 2 clearly show the dramatic effect of multiple Fourier horns on the electrical drive power

required for atomization. Clearly, in terms of electrical drive power, the optimum number of Fourier horns is 3 or 4. As mentioned previously, both 3- and 4-Fourier horn nozzles were fabricated and studied, and their atomization performances were found to be very similar. Since there is no advantage in further increase in the number of Fourier horns, new nozzles with 5 or more Fourier horns were not fabricated. Only the 1.0 MHz nozzles with a central channel consisting of one, two, three, and four Fourier horns were fabricated earlier in the study to verify the essential requirement of peak vibration displacement on the nozzle endface for initiation of temporal instability of Faraday waves and atomization. The dramatic effect of multiple Fourier horns on the electrical drive power required for initiation of atomization was clearly demonstrated by comparing the measured drive power required for nozzles with one to four Fourier horns. We found that while the 3- and 4-Fourier horn nozzles readily produced atomization with electrical drive power significantly below 0.1 W at throughput of 100 μl min^{-1}, the 2-Fourier horn nozzle required a drive power of 0.6 W to initiate atomization. In contrast, no atomization could be initiated with the 1-Fourier horn nozzle even at a drive power as high as 0.8 W.

V. Ideal device for inhalation drug delivery

Monodisperse droplets <10 μm in diameter are highly desirable in many biomedical and pharmaceutical applications.[35,36] For pulmonary microcirculation-related applications, the droplets must be smaller than 7 μm in diameter to safely pass through the micro vessels of the lung without causing obstruction.[37] Monodisperse droplets 3 to 5 μm are ideal to efficiently target medications to the respiratory system depending on the disease and its site.[38] 1–3 μm droplets (optimal at 2 μm) are ideal for delivery of medications to the alveolar capillary bed for maximum systemic absorption.[38,39] Inhalation is an attractive route for non-invasive delivery of drugs,[40–43] especially peptides and proteins that are easily broken down by enzymes in the stomach when taken orally.[42,43] Current commercial devices (*i.e.*, nebulizers, metered dose and dry powder inhalers) suffer from broad droplet size distributions and low throughput, which make it difficult to deliver sufficient dosages of drugs precisely and rapidly to targeted sites. Even piezoelectric-driven membrane systems, the most efficient devices presently available, provide only moderate throughput ranging from 160 to 400 μl min^{-1} of polydisperse droplets or aerosols. Recent *in vivo* studies have indicated that in both children and adults, when inhaling typical aerosols from current commercial devices, the upper airways,[44] ventilator, and endotracheal tubes are significant barriers to lung deposition.[45] As a direct result of polydisperse droplet size distributions, drugs are delivered to non-targeted sites, resulting in harmful side effects in the pharynx and losses in the ventilator/endotracheal tubes. Thus, there is a need for a miniaturized device that produces monodisperse droplets of the optimum size range of 1–5 μm. Ideally, such a device must also have high throughput to reduce treatment time, minimal ballistic effect to reduce deposition on the pharynx, small physical size, and low electrical drive power that can be supplied by a battery. Devices based on the new ultrasonic nozzle architecture and design reported here may fill this important biomedical need.

To test applicability of the ultrasonic droplet generators to pulmonary drug delivery, two preliminary experiments were carried out earlier using a 1.0 MHz nozzle with a central channel.[29] In the first experiment, a silastic reproduction of the human upper airway (mouth, pharynx, and larynx)[46] was used as the upper airway model in the deposition of isoproterenol monodisperse aerosols under simulated conditions of 3-litre tidal volume of ambient air in one breath. The total drug recovery measured ranges from 90 to 95%, and 70% of the administered dose was delivered to the lower airways.[29] The percentage delivered to the lower airways increased by 10% as the droplet diameter was reduced from 4.5 μm to 3.5 μm. In the second experiment, human recombinant insulin R-100 (diluted with equal amount of a buffer solution)[47] was atomized. The atomized insulin was found to retain its biological activity.[29] Thus, a higher efficiency of delivery to the lower airways can be expected using the monodisperse medicinal droplets or aerosols of smaller diameter produced by the new ultrasonic droplet generators at frequency higher than 1.0 MHz.

VI. Conclusions and remarks

Using the classical model geometry facilitated by the simple architecture of silicon-based multiple-Fourier horn ultrasonic nozzles, we verified unequivocally temporal instability of Faraday waves at MHz frequency as the mechanism for atomization and generation of micrometre monodisperse droplets. The new MHz nozzles employ external liquid feeding and produce fine sprays of 2.2 to 4.6 μm monodisperse droplets with minimal ballistic effect at high throughput (420 μl min^{-1}) and very low electrical drive power (80 mW). The measured droplet diameters and drive power are verified by the theoretical formula based on Rayleigh oscillation and the critical vibration displacements predicted with the temporal instability of Faraday waves, respectively. These centimetre-sized new nozzles require much simpler fabrication steps and significantly lower electrical drive power than earlier nozzles with a central channel. Furthermore, a large number of nozzles with similar or different design specifications can be readily fabricated in one batch on a common silicon wafer. This will drastically reduce the costs of fabrication. Thus, these miniaturized MHz ultrasonic droplet generators, when further integrated and packaged using existing microelectronics technology, should provide the basis for viable devices for inhalation drug delivery.

Other potential applications of the high-throughput droplet generators include delivery of lipid-based micro-encapsulated biological entities[48] or therapy,[49] nanoparticles synthesis,[50] 3-D coating, and nano-electronic and -photonic device processing. For the last application, spray coating of soft micrometre monodisperse droplets of processing materials such as photoresists using the droplet generator may be employed to replace the present spin-coating technique to alleviate agglomeration of photoresist over 3-D nanostructures due to spinning of the device substrate.

Acknowledgements

The financial support by the National Institute of Health (NIH/NIBIB), USA under Grant 5R21EB006366 is gratefully acknowledged.

References

1 S. A. Elrod, B. Hadimioglu, B. T. Khuri-Yakub, E. G. Rawson, E. Richley and C. F. Quate, *J. Appl. Phys.*, 1989, **65**, 3441–3447.
2 D. Huang and E. S. Kim, *J. Microelectromech. Syst.*, 2001, **10**, 442–449; Q. F. Zhou, C. Sharp, J. M. Cannata, K. K. Shung, G. H. Feng and E. S. Kim, *Appl. Phys. Lett.*, 2007, **90**, 113502.
3 G. G. Perçin, G. G. Yaralioglu and B. T. Khuri-Yakub, *Rev. Sci. Instrum.*, 2002, **73**, 4385–4389.
4 B. de Heji, B. van der Schoot, H. Ho, J. Hess and N. F. de Rooij, *Sens. Actuators, A*, 2000, **85**, 430–434.
5 J. M. Meacham, C. Ejimofor, S. Kumar, F. L. Degertekin and A. G. Fedorov, *Rev. Sci. Instrum.*, 2004, **75**, 1347–1352.
6 J. M. Meacham, M. J. Varady, F. L. Degertekin and A. G. Fedorov, *Phys. Fluids*, 2005, **17**, 100605.
7 V. G. Zarnitsyn, J. M. Meacham, M. J. Varady, C. Hao and A. G. Fedorov, *Biomed. Microdevices*, 2008, **10**, 299–308.
8 A. Qi, J. R. Friend, L. Y. Yeo, D. A. V. Morton, M. P. McIntosh and L. Spiccia, *Lab Chip*, 2009, **9**, 2184–2193.
9 N. Maehara, S. Ueha and E. Mori, *Rev. Sci. Instrum.*, 1986, **57**, 2870–2876.
10 K. M. G. Taylor and O. N. M. McCallion, *Int. J. Pharm.*, 1997, **153**, 93–104.
11 M. Faraday, *Philos. Trans. R. Soc. London*, 1831, **A52**, 299–340.
12 B. Rayleigh, *Philos. Mag.*, 1883, **16**(5), 50–58.
13 J. Miles and D. Henderson, *Annu. Rev. Fluid Mech.*, 1990, **22**, 143–165.
14 G. S. Guthart and T. Yao-tsu. Wu, *Proc. R. Soc. London, Ser. A*, 1991, **434**, 435–440.
15 K. Kumar, *Proc. R. Soc. London, Ser. A*, 1996, **452**, 1113–1126.
16 E. A. Cerda and E. L. Tirapegui, *Phys. Rev. Lett.*, 1997, **78**, 859–862.
17 C. L. Goodridge, H. G. E. Hentschel and D. P. Lathrop, *Phys. Rev. Lett.*, 1999, **82**, 3062–3065.
18 A. J. Yule and Y. AL-Suleimani, *Proc. R. Soc. London, Ser. A*, 2000, **456**, 1069–1085.
19 S. C. Tsai, Y. L. Song, C. S. Tsai, Y. F. Chou and C. H. Cheng, *Appl. Phys. Lett.*, 2006, **88**, 014102, (also *Virt. J. Nanoscale Sci. Technol.*, Jan. 16, 2006).
20 S. C. Tsai, C. H. Cheng, N. Wang, Y. L. Song and C. S. Tsai, *IEEE Trans. Ultrason. Ferroelectr. Freq. Control*, 2009, **56**(9), 1968–1979.
21 S. C. Tsai, P. Luu, P. Childs and C. S. Tsai, *IEEE Trans. Ultrason. Ferroelectr. Freq. Control*, 1999, **46**, 139–146.
22 B. Rayleigh, *Theory of Sound*. 2nd ed. vol. 2: Dover Publications, Inc., New York, 343–349 (1945).
23 B. Rayleigh, *Proc. R. Soc. London*, 1879, **29**, 71–97.
24 E. Eisner, *J. Acoust. Soc. Am.*, 1963, **35**, 1367–1377.
25 S. C. Tsai, Y. L. Song, T. K. Tseng, Y. F. Chou, W. J. Chen and C. S. Tsai, *IEEE Trans. Ultrason. Ferroelectr. Freq. Control*, 2004, **51**, 277–286.
26 A. Lal and R. M. White, *Proc. IEEE Ultrasonics Symposium*, 1996, **1**, 339–342.
27 J. D. Bassett and A. W. Bright, *J. Aerosol Sci.*, 1976, **7**, 47–51.
28 S. C. Tsai, P. Luu, P. Childs, A. Teshome and C. S. Tsai, *Phys. Fluids*, 1997, **9**, 2909–2918.
29 S. C. Tsai, R. W. Mao, D. Mukai, S. K. Lin, A. F. Wilson, N. Wang, M. Brenner, S. C. George, J. Y. Yang, P. Wang, and C. S. Tsai, *International Conference on Accelerating Biopharmaceutical Development*, Coronado, CA, March 9, 2009.
30 S. C. Tsai, Y. L. Song, Y. F. Chou, G. Qiu, E. Degiovanni, N. Wang, C. H. Cheng, and C. S. Tsai, *Proc. NSTI Nanotechnology Conference and Trade Show*, Anaheim, CA, May 8–12, 2005.
31 O. S. Usmani, M. F. Biddiscombe and P. J. Barnes, *Am. J. Respir. Crit. Care Med.*, 2005, **172**, 1497–1504.
32 A. L. Coates, M. Green, K. Leung, J. Chan, N. Ribeiro, E. Louca, F. Ratjen, M. Charron, M. Tservistas and M. Keller, *Pediatr. Pulmonol.*, 2008, **43**, 753–759.
33 B. L. Rottier, C. J. P. van Erp, T. S. Sluyter, H. G. M. Heijerman, H. W. Frijlink and A. H. de Boer, *Journal of Aerosol Medicine and Pulmonary Drug Delivery*, 2009, **22**, 263–269.
34 F. Barreras, H. Amaveda and A. Lozano, *Exp. Fluids*, 2002, **33**, 405–413.
35 P. Garstecki, M. J. Fuerstman, H. A. Stone and G. M. Whitesides, *Lab Chip*, 2006, **6**, 437–446.
36 H. A. Stone, A. D. Stroock and A. Ajdari, *Annu. Rev. Fluid Mech.*, 2004, **36**, 381–411.
37 K. Hettiarachchi, E. Talu, M. L. Longo, P. A. Dayton and A. P. Lee, *Lab Chip*, 2007, **7**, 463–468.
38 J. S. Patton and P. R. Byron, *Nat. Rev. Drug Discovery*, 2007, **6**, 67–74.
39 J. Heyder, *Proc. Am. Thorac. Soc.*, 2004, **1**, 315–320.
40 R. Langer, *Science*, 2001, **293**, 58–59.
41 D. A. LaVan, T. McGuire and R. Langer, *Nat. Biotechnol.*, 2003, **21**, 1184–1191.
42 D. A. Edwards, J. Hanes, G. Caponetti, J. Hrkach and R. Langer, *Science*, 1997, **276**, 1868–1871.
43 R. Langer and N. A. Peppas, *AIChE J.*, 2003, **49**, 2990–3006.
44 S. Sangwan, R. Condos and G. C. Smaldone, *J. Aerosol Med.*, 2003, **16**, 379–386.
45 T. G. O'Riordan, K. Hughes and G. C. Smaldone, *Respir. Care*, 1994, **39**, 1162–1168.
46 A. F. Wilson, D. S. Mukai and J. J. Ahdout, *Am. Rev. Respir. Dis.*, 1991, **143**, 1034–1037.
47 H. C. Lai, T. J. Liu, C. T. Ting, J. Y. Yang, L. Huang, D. Wallace, P. Kaiser and P. H. Wang, *Am. J. Physiol.: Endocrinol. Metab.*, 2007, **292**, E292–7.
48 Shia-Yen Teh and A. P. Lee, *Proc. 13th Inter.Conf. on Miniaturized Systems for Chemistry and Life Sciences, μTAS*, 2009, pp. 1353–1355.
49 J. Heyes, L. Palmer, K. Chan, C. Giesbrecht, L. Jeffs and I. MacLachlan, *Mol. Ther.*, 2007, **15**, 713–720.
50 S. C. Tsai, Y. L. Song, C. S. Tsai, C. C. Yang and W. Y. Chiu, *J. Mater. Sci.*, 2004, **39**, 3647–3657.